NAR Breakthrough Article

H2A.Z is dispensable for both basal and activated transcription in post-mitotic mouse muscles

Edwige Belotti[1], Nicolas Lacoste[1], Thomas Simonet[1], Christophe Papin [ID][2],
Kiran Padmanabhan[3], Isabella Scionti[1], Yann-Gaël Gangloff [ID][1], Lorrie Ramos[4],
Defne Dalkara[4], Ali Hamiche [ID][2,†], Stefan Dimitrov[4,5,†] and Laurent Schaeffer [ID][1,6,*,†]

[1]Institut NeuroMyoGène, Université Claude Bernard Lyon 1, Université de Lyon, INSERM U1217, CNRS UMR5310, 8 avenue Rockefeller, 69008 Lyon, France, [2]Institut de Génétique et de Biologie Moléculaire et Cellulaire, CNRS/INSERM/ULP, Parc d'innovation, 1 rue Laurent Fries, 67404 Ilkirch Cedex, France, [3]Institut de Génomique Fonctionnelle de Lyon, CNRS UMR 5242, École Normale Supérieure de Lyon, Université Claude Bernard Lyon 1, 32-34 Avenue Tony Garnier, 69007 Lyon, France, [4]Institute for Advanced Biosciences (IAB), Université Grenoble Alpes, CNRS UMR 5309, INSERM U1209, Site Santé - Allée des Alpes, 38700 La Tronche, France, [5]Izmir Biomedicine and Genome Center, Dokuz Eylul University Health Campus, Balcova, Izmir 35330, Turkey and [6]Centre de Biotechnologie Cellulaire, Hospices Civils de Lyon, Lyon, France

ABSTRACT

While the histone variant H2A.Z is known to be required for mitosis, it is also enriched in nucleosomes surrounding the transcription start site of active promoters, implicating H2A.Z in transcription. However, evidence obtained so far mainly rely on correlational data generated in actively dividing cells. We have exploited a paradigm in which transcription is uncoupled from the cell cycle by developing an *in vivo* system to inactivate H2A.Z in terminally differentiated post-mitotic muscle cells. ChIP-seq, RNA-seq and ATAC-seq experiments performed on H2A.Z KO post-mitotic muscle cells show that this histone variant is neither required to maintain nor to activate transcription. Altogether, this study provides *in vivo* evidence that in the absence of mitosis H2A.Z is dispensable for transcription and that the enrichment of H2A.Z on active promoters is a marker but not an active driver of transcription.

INTRODUCTION

Histone variants are non-allelic isoforms of conventional histones (1,2). Each histone has variants, though H4 variants are only found in hominids (1,3,4). Histone variants differ from conventional histones in their primary sequence, transcriptional regulation and timing of expression during the cell cycle (1–3). Incorporation of histone variants can confer novel structural properties to nucleosomes and change the functional chromatin landscape (3,5–7). The current view is that histone variants are involved in all aspects of DNA metabolism including transcription, replication and repair (1) and that they can be implicated in numerous diseases, particularly in cancer (for review see (8–10)).

The H2A family of histone variants is one of the largest. In addition to conventional H2A, the family comprises of at least macroH2A, H2A.X, H2A.Z and H2A.Bbd (11).

In mammals, H2A.Z is encoded by two genes, H2A.Z-1 and H2A.Z-2, located on chromosomes 3 and 11. H2A.Z-1 and H2A.Z-2 differ by only three amino-acids (12,13). H2A.Z is an essential protein in mammals (14). ANP32E and YL1 are part of large protein complexes that were identified as H2A.Z specific chaperones, responsible for either its eviction or its deposition in chromatin (15,16). In vertebrates, genome-wide studies have shown that H2A.Z is enriched at active promoters (17–19), in facultative heterochromatin (20) and at centromeres (21,22). Interestingly, at the +1 and –1 nucleosome positions surrounding the Transcription Start Site (TSS), H2A.Z proportions are correlated with the strength of transcription (18,23).

H2A.Z is also preferentially bound to other regulatory elements such as enhancers and CTCF-binding sites, which

---

mark insulator sites in the genome, and more generally in chromatin regions where histones have a high turnover (15,17,18,24–26). From all these observations, it appears that H2A.Z could be a key player in the control of transcription.

However, the data linking H2A.Z-containing nucleosomes and transcription remain mainly correlative, and based on studies carried out in cultured cells. Their interpretation has to take into account perturbations of DNA replication and cell division that can indirectly affect gene expression. For example, depletion of H2A.Z in vertebrates results in strong mitotic and cytokinesis defects and can activate an apoptotic program leading to cell death (27). H2A.Z is enriched at early replication origins and participates to their activation (28,29). It appears that unravelling the exact function of H2A.Z in the control of transcription requires a system in which H2A.Z can be inactivated in cells that no longer replicate DNA. Skeletal muscle and the Cre-/loxP system provide such a paradigm.

Transgenic mice, expressing the Cre recombinase under the control of the human α-skeletal actin promoter (HSA-Cre), express the recombinase in post-mitotic skeletal muscle cells (30). Thus, breeding HSA-Cre mice with H2A.Z-1$^{flox/flox}$:H2A.Z-2$^{flox/flox}$ mice specifically inactivates H2A.Z-1 and H2A.Z-2 in post-mitotic skeletal muscle cells (hereafter named H2A.Z dKO). These cells provide a convenient tool to analyse *in vivo* the requirement of H2A.Z for transcription maintenance and regulation.

Gene expression in skeletal muscle cells is tightly controlled by innervation. Two days after denervation, muscle cells have adopted a new gene expression program involving the activation and the repression of hundreds of genes (31). The best characterized genes activated upon denervation encode a variety of proteins: transcription factors (MYOD, Myogenin), neurotransmitter receptors (acetylcholine receptor subunits), kinases (MuSK, PAK1), histone deacetylases (HDAC6, HDAC4) and ubiquitin ligases (MURF1, MAFBX, MUSA1) (31–33). Depriving muscles of their innervation thus provides a convenient method to evaluate the involvement of H2A.Z in *de novo* regulation of gene expression.

Our RNA-seq and ATAC-seq analysis of innervated and denervated H2A.Z dKO muscles revealed that the absence of H2A.Z affected neither steady state nor activated gene expression.

MATERIALS AND METHODS

Generation of H2A.Z-1/H2A.Z-2 HSA-Cre mice

The H2A.Z mouse line was generated at the 'Institut Clinique de la Souris' (ICS-MCI; Illkirch, France). The targeting vector containing a Frt Neomycin resistance cassette and (i) *H2afz*: in which exons 2–4 was flanked by loxP sites or (ii) *H2afv*: in which exons 4–5 was flanked by loxP sites was generated. Each constructs were electroporated into mouse embryonic stem (ES) cells. Targeted ES cells were injected into C57BL/6 blastocysts which were implanted in pseudo-pregnant females. Removal of the Neomycin cassette in the targeted allele was accomplished by crossing the chimeric males giving germline transmission with Flp

transgenic females to generate mice with the conditional allele (Figure 1A and B). Each strain was backcrossed for 10 generations on C57BL/6N mice. Finally, H2A.Z-1$^{flox/flox}$:H2A.Z-2$^{flox/flox}$ mice were obtained by crossing the mice with HSA-Cre transgenic strain (30) to generate the muscle specific conditional double KO. Mice were genotyped by PCR amplification of genomic DNA extracted from newborn biopsies. A 40 μl volume of extraction buffer (0.5 mg/ml proteinase K, 0.2% SDS, 0.2 M NaCl, 100 mM Tris, 5 mM EDTA, pH 8.0) was added to biopsies and incubated at 54 °C overnight. After DNA precipitation and resuspension in 200 μl of water, 1 μl of DNA was taken as template in a 25 μl PCR reaction using the Go Taq DNA polymerase (Promega) according to the provider's recommendation. Genotyping was performed with primers listed in Supplementary Table S1.

Cell culture

Mouse embryonic fibroblasts (MEFs) were derived from E13.5 WT and double H2A.Z flox embryos. Heads and internal organs were removed, the torso was minced into chunks of tissue. Cells were immortalized with a retrovirus expressing the large SV40 T antigen and cultured in high glucose Dulbecco's modified Eagle's medium (DMEM), with sodium pyruvate, Glutamax (Gibco), 10% fetal bovine serum (FBS), and penicillin–streptomycin in a humidified incubator at 37°C and a 5% CO_2 atmosphere. Immortalized H2A-Z.1$^{flox/flox}$:H2A-Z.2$^{flox/flox}$ MEFs were plated at 30% of confluency and were infected with recombinant adenoviruses encoding either GFP or a Cre-GFP fusion (Ad-CMV-GFP or Ad-CMV-Cre-GFP, Vector Biolabs, Philadelphia, Pennsylvania, USA) to respectively generate control (CTL) and H2A.Z double KO (H2A.Z dKO) cell lines. Viruses were diluted in the culture media for overnight infection. Cells were then washed and were diluted 4 times every 2 days to have them always below a confluence of 70%. Cells were collected every 2 days until 8 days after infection.

Mice care

Animals were provided with mouse chow and water *ad libitum* in a restricted-access, specific pathogen–free animal care facility at the Ecole Normale Supérieure of Lyon (Plateau de Biologie Expérimentale de la Souris). All procedures were performed in accordance with national and European legislation on animal experimentation.

Denervation of hindlimb muscles

Section of the left sciatic nerve was used to induce denervation. Briefly, after the mice were anesthetized with an intraperitoneal injection of ketamine (100 mg.kg^{-1}) and xylazine (10 mg.kg^{-1}), the sciatic nerve was exposed in the thigh and doubly cut (5 mm apart) just distal to the sciatic notch. Contralateral muscles that were not operated and were used as controls. Forty eight hours post-denervation, non-denervated and denervated *tibialis anterior* (TA) muscles were collected and snap frozen in liquid nitrogen. All
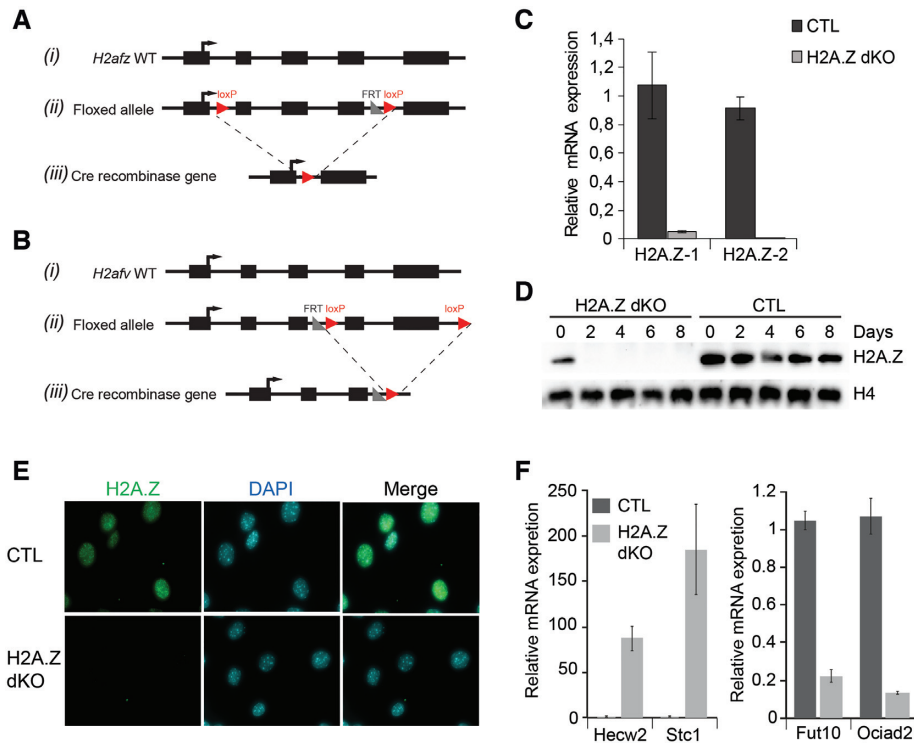
Figure 1. Generation and characterisation of the H2A.Z-1 and H2A.Z-2 models. (**A**) (i) Wild-type *H2afz* gene structure. Black boxes indicate the exons. (ii) The conditional allele of the *H2afz* flox/flox gene. LoxP sites were inserted at the indicated position. (iii) Organization of the H2A.Z-1 knock-out (KO). Exons 2, 3 and 4 are deleted upon expression of Cre recombinase to generate the KO allele *H2afz* (−/−). (**B**) Same as (A), but for the *H2afv* gene. LoxP site was inserted on both ends of exon 4–5. After Cre-recombinase expression, exon 4 and 5 are deleted to create the KO allele *H2afv* (−/−). (**C**) Bar graphs representing the expression level of *H2afz* and *H2afv* genes measured by RT-qPCR analysis in MEFs infected with either control adenovirus or with adenovirus expressing Cre recombinase. (**D**) H2A.Z is efficiently depleted upon infection of MEFs with adenovirus expressing Cre recombinase. Western blot of MEF cells using anti-H2A.Z antibody. H4 was used as loading control. (**E**) Immunofluorescence detection of H2A.Z on proliferating MEFs 2 days after infection. (**F**) RT-qPCR of RNA isolated from CTL and H2A.Z double flox MEF cells in absence or presence of adeno-Cre virus particles. On the left panel, some up-regulated genes in absence of H2A.Z and on the right panel some down-regulated genes in absence of H2A.Z.

operative procedures were performed using aseptic techniques and according to the ethical committee recommendations (Ceccap-ENS-2014-019).

Quantitative RT-PCR

For RNA extraction from MEF cells, 1 ml of TRI reagent (Sigma) was added to 10 cm cell culture plate that have been washed once before with PBS. Cells are then scrapped and place in a 1.5 ml tube and processed following provider's instructions. To extract total RNA from muscles, 500 μl of TRI Reagent (Sigma) was added to individual frozen *tibialis anterior* in tubes containing ceramics beads (Lysing Matrix D – MP biomedicals) for homogenization in a Pre-Cellys (Bertin Technologies) (6500 RPM, 3 × 10 s). After centrifugation, TRI Reagent was removed and beads were washed once with 500 μl of TRI reagent. Total RNA was extracted following provider's instruction. To generate cDNA, total RNA was treated with DNase (Ambion) and reverse transcribed with RevertAid H Minus Reverse Transcriptase (ThermoFisher) primed with random hexamers. RT-qPCR was performed using SYBR Green Mastermix (Qiagen) in the CFX-connect system (Bio-Rad). Relative expression levels were normalized to *GusB* and *Rpl41* housekeeping genes expression using the $\Delta\Delta C_t$ method. Primers are listed in Supplementary Table S2.

RNA-seq

Total RNA from the *tibialis anterior* muscle was extracted from three different mice. Libraries of template molecules suitable for strand-specific high-throughput RNA sequencing were created using a TruSeq Stranded Total RNA with Ribo-Zero Gold Prep Kit (RS-122-2301; Illumina) as previously described (34). The libraries were sequenced on Illumina Hiseq 4000 sequencer as single-end 50 bp reads following Illumina's instructions. Image analysis and base calling were performed using RTA 2.7.3 and bcl2fastq 2.17.1.14. Adapter dimer reads were removed using DimerRemover v0.9.2. Reads were mapped to the mouse genome (mm9) using Tophat (35) v2.0.14 and Bowtie (36) v2-2.1.0. Quantification of gene expression was performed using HTSeq (37) v0.6.1 and gene annotations from Ensembl release 67.

Nuclei preparation

Muscles of individual hind limbs were collected and put in 4 ml of cold buffer A (300 mM sucrose, 10 mM NaCl, 1.5 mM MgCl₂, 15 mM Tris–HCl pH 8.0 and protease inhibitor cocktail (Sigma)). Muscles were minced with scissors and transfered in a dounce homogenizer where 50 strokes of the loose pestle were slowly applied. The extract was then passed through a 100 μm cell strainer to remove myofibrils

debris and placed back into a clean cold dounce homogenizer. Nonidet P-40 was then added to the extract to a final concentration of 0.5%, which was then incubated for 15 min at 4°C. Subsequently, 50 strokes with the tight pestle were applied. The nuclei suspension was finally clarified through a 40 μm cell strainer, centrifuged at 2000 g for 10 min at 4°C and washed in cold buffer A. Purified nuclei were resuspended in a small volume of buffer A for further ChIP-seq, ATAC-seq or immunoblot analysis.

ChIP-seq

Muscle nuclei from three different mice were pooled to perform the ChIP-seq experiment. Purified nuclei were crosslinked with 0.2% formaldehyde for 1 min before quenching with 125 mM glycine for 5 min at room temperature. The buffer was then changed to 300 mM NaCl, 300 mM sucrose 0.1% NP-40, 2 mM $CaCl_2$, 15 mM Tris–HCl pH 8.0 following a centrifugation at 2000 g for 10 min. MNase (Roche diagnostic) was then added to the nuclei and incubated at 37°C for a period of time long enough to generate a majority of mono- and di-nucleosomes. The reaction was stopped by increasing EDTA concentration to 10 mM. After a 5 min centrifugation at 20 000 g, 20 μg of chromatin from the supernatant were incubated overnight at 4°C with an immunopurified highly specific polyclonal anti-H2A.Z rabbit antibody generated in-house (15), followed by 2 h incubation with Protein A dynabeads (Invitrogen). Immunoprecipitated material was sequentially washed with buffer containing low salt (150 mM NaCl), high salt (500 mM NaCl) and finally a high stringency wash (500 mM NaCl, 0.25 M LiCl and 1% sodium deoxycholate) in 10 mM Tris–HCl pH 8, 1 mM EDTA buffer. DNA was released from immunoprecipitated complexes by overnight incubation at 65°C and finally isolated over Qiagen PCR purification columns.

Libraries were prepared using the Diagenode MicroPlex Library Preparation kit v2, and sequenced on Illumina Hiseq 4000 sequencer as single-end 50 bp reads following Illumina's instructions. Image analysis and base calling were performed using RTA 2.7.3 and bcl2fastq 2.17.1.14. Adapter dimer reads were removed using DimerRemover v0.9.2. Reads were mapped to the mouse genome (mm9) using Bowtie v1.0.0 with the following arguments: -m 1 –strata –best -y -S –l 40 -p 2.

ATAC-seq

Purified nuclei are quantified using DAPI and 50 000 of them are taken to performed the ATAC-seq protocol as described in Buenrostro *et al.* (38). Nextera adapters were trimmed from reads with Trimmomatic (39). Remaining paired reads longer than 20 bp were mapped to the mouse genome (mm9) using Bowtie, using the local alignment mode (–local) and a maximum fragment length set to 2000 bp (–maxins).

Immunoblot

Chromatin preparations were separated on a 18% SDS-PAGE and transferred onto polyvinylidene fluoride (PVDF) Immobilon-P membranes (Millipore). Immunoblots were performed with enhanced chemiluminescence (ECL) PLUS reagent (GE Healthcare) according to the manufacturer's instructions. Antibodies used were as follows: rabbit monoclonal anti-Histone H4 pan (04-858, Merck Millipore); rabbit polyclonal anti-H3 (#61277); mouse monoclonal anti-α-Tubulin (T6074, Sigma); the rabbit polyclonal anti-H2A.Z (15).

Histology

Hind limb muscles surrounding the tibial bone (Gastrocnemius, Plantaris, Soleus (GPS), TA and Extensor Digitorum Longus (EDL) were collected from 7 weeks-old CTL and H2A.Z dKO mice, frozen in isopentane cooled on dry ice, and cross-sectioned at 10 μm thickness in a cryostat. Transverse sections were stained with Hematoxylin and Eosin for immunohistochemistry and with Wheat Germ Agglutinin (WGA) / DAPI for immunofluorescence, analysed using an Axio Scan.Z1 slide scanner (Zeiss Microscopy). Morphometrics analysis were performed with the ImageJ software.

Immunofluorescence

Cross sections were rehydrated in PBS, fixed with 4% PFA for 10 min, permeabilized in 1× PBS, 0.1% Triton for 30 min at room temperature then saturated in 1× PBS 1% BSA 1% normal goat serum for 1 h. Staining with green WGA (W11261, Molecular Probes) and DAPI were performed overnight at 4°C. Coverslips were then mounted with Vectashield (Vector Laboratories) and sealed with nail polish.

For myofibers staining, an EDL muscle was collected and fixed in 4% paraformaldehyde 10 min for tissue dissection and staining. Muscles were slowly teased with fine forceps to isolate individual fibers and small fiber bundles. Fibers were permeabilized in 1× PBS, 0.1% Triton for 30 min at room temperature, saturated in 1× PBS 1% BSA for 1 h before overnight incubation with the primary antibody (home-made anti-H2A.Z 1/100) diluted in blocking buffer. After washing, fibers were incubated with a secondary antibody conjugated with FITC (Molecular probes). DNA and neuromuscular junctions were respectively stained with DAPI (2 μg/ml) and α-bungarotoxin Alexa-555 (Molecular probes) for 2 h at room temperature. After washing, fibers were mounted on glass slide with Vectashield (Vector Laboratories) and analysed using a confocal laser scanning microscope (Leica SP5). Images were processed using ImageJ software.

Computational analyses

Repeat analyses of RNA-seq and ChIP-seq datasets were performed as previously described (35). Processed datasets were restricted to repeat families with >500 mapped reads per ChIP sample or >5 reads per million mapped reads per RNA sample to avoid over- or under-estimating fold enrichments due to low sequence representation.

Heatmaps and quantitative analysis of the ChIP-seq data were performed using seqMINER (http://bips.u-strasbg.fr/seqminer/). As reference coordinates, we used the Ensembl 67 database of the mouse genome (mm9).

For ATAC-seq data not properly paired, supplementary alignments and putative PCR duplicates were removed using the Picard Tools (https://broadinstitute.github.io/picard/) (39–41). Enriched regions were identified with MACS2 (42) at q value 0,01, with either a wide or narrow assumption of how accessibility is inferred from fragments ends: a wide model was a half nucleosome length (73bp) centered on the fragment ends (ie –nomodel –shift −37 –extsize 73), these ends having been shifted 4bp forward for (+) reads and 5bp backward for (−) reads, in order to represent the center of the tn5 transposon binding event, as suggested (43); the narrow model was the tn5 transposon occupancy only (ie –nomodel –shift -5 –extsize 9). Mitochondrial peaks and peaks overlapping blacklisted regions were filtered out (44). In order to compare accessibility between both conditions, we focused on the union of their peaks, analysing those called with the wide or narrow model separately. As an example, for the peaks produced with the wide calling model, we first defined true enriched regions in each condition as MACS2 peaks shared by the three replicates, taking the union of the intervals, if overlapped by at least 25% of their length; we then merged these true enriched regions from both conditions, taking the union of regions overlapping by more than 50% of their length, or keeping not overlapped regions with their boundaries unchanged (45). We quantified the fragments ends tn5-shifted and 37 bp extended falling within these 52 142 union intervals. Differential peak enrichment was then computed using DESeq2 (46), Heatmaps were performed using deeptools2 (47), plotting the means of the fold enrichment files generated by MACS2 from the three replicates for each condition, using the narrow peak calling, the TSSs being sorted either by the RNA-seq expression data from the CTL condition, or by the CTL ATAC-seq TSS enrichment.

RESULTS

Ablation of H2A.Z-1 and H2A.Z-2 in MEFs cells

The H2A.Z-1$^{flox/flox}$:H2A.Z-2$^{flox/flox}$ mouse line was created with the strategy described in Figure 1A and B. Briefly, loxP sequences were inserted before exon 2 and after exon 4 of *h2afz* (H2A.Z-1) and before exon 4 and after exon 5 of *h2afv* (H2A.Z-2) using the standard recombination strategy. To evaluate the efficacy of our inactivation strategy and the stability of H2A.Z, we first isolated Mouse Embryonic Fibroblast (MEF) cell lines from the double floxed mouse line. Upon Cre induction using an adenoviral system, *h2afz* and *h2afv* knock-down was evaluated by RT-qPCR (Figure 1C), and H2A.Z protein depletion was evaluated by western blotting (Figure 1D) and immunofluorescence (Figure 1E). Two days after infection by the adeno-Cre, H2A.Z protein was already undetectable in cycling cells. H2A.Z dKO cells did not survive >9 days after H2A.Z withdrawal, recapitulating the essential function of H2A.Z (27). We then used RT-qPCR to evaluate the expression of a set of genes known to be affected by the absence of H2A.Z in mouse cells (25). As expected, they were misregulated in the absence of H2A.Z (Figure 1F). We then initiated the study of the role of H2A.Z in post-mitotic muscle cells *in vivo* to determine if, in absence of replication and cell division, the same effects would be observed.
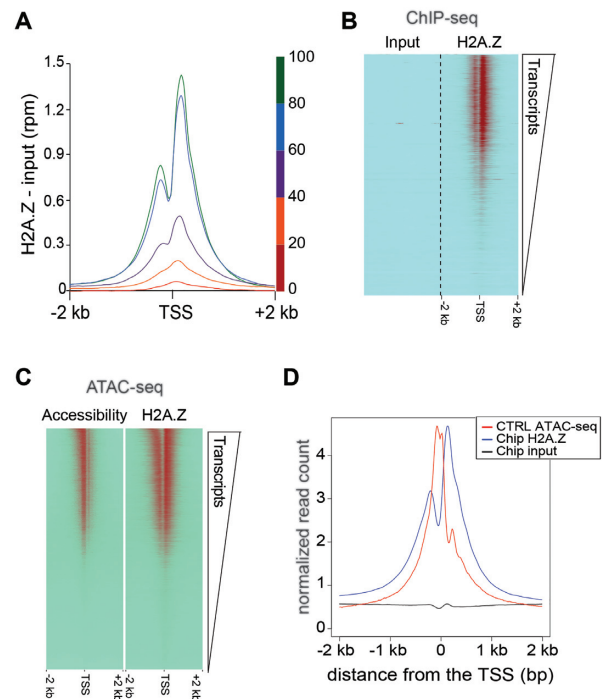

Figure 2. H2A.Z localisation and DNA accessibility at genome-wide level according to the transcription. (**A**) Distribution of H2A.Z relative to the transcription start sites (TSS) (the distinct colors indicate the different levels of transcription) and (**B**) Heat map of input and H2A.Z ChIP-seq enrichments around the transcription start sites (TSSs) ranked according to the RNA-seq levels, in muscle skeletal myofibers. (**C**) Heat map of the ATAC-seq signal and H2A.Z Chip-seq enrichment around the transcription start sites (TSSs) ranked according the RNA-seq levels. (**D**) Distribution of H2A.Z and DNA accessibility relative to the TSS.

H2A.Z is enriched at TSS of active genes in mouse skeletal muscle

Currently, no data are available on the distribution of H2A.Z *in vivo* in skeletal muscle and more generally in post-mitotic cells. To analyse the genomic distribution of H2A.Z in adult skeletal muscle, ChIP-seq was performed on *tibialis anterior* (TA) muscles from 7 weeks old mice. Results indicated that H2A.Z was enriched around transcriptional start sites (TSS) as in most other cell types (48) (Figure 2A). RNA-seq was then performed to compare gene expression data to the ChIP-seq. The results showed that the abundance of H2A.Z was correlated with gene expression (Figure 2B)**.** Altogether, these results are in agreement with numerous previous studies showing that H2A.Z is enriched around the TSS of active genes (15,17,18). Skeletal muscle thus provides an adequate system to evaluate the requirement of H2A.Z for gene expression in post-mitotic cells.

Using ATAC-seq in control muscles to assess chromatin accessibility at the genome level, we could readily detect a correlation between the presence of H2A.Z and accessible regions of the DNA (Figure 2C). Since ChIP-seq experiments showed a correlation between the strength of transcription and H2A.Z enrichment at the TSS, we can conclude that in muscle cells, as in any cell type, a correlation exists between transcription strength and chromatin accessibility. ChIP-seq and ATAC-seq alignment further indicated
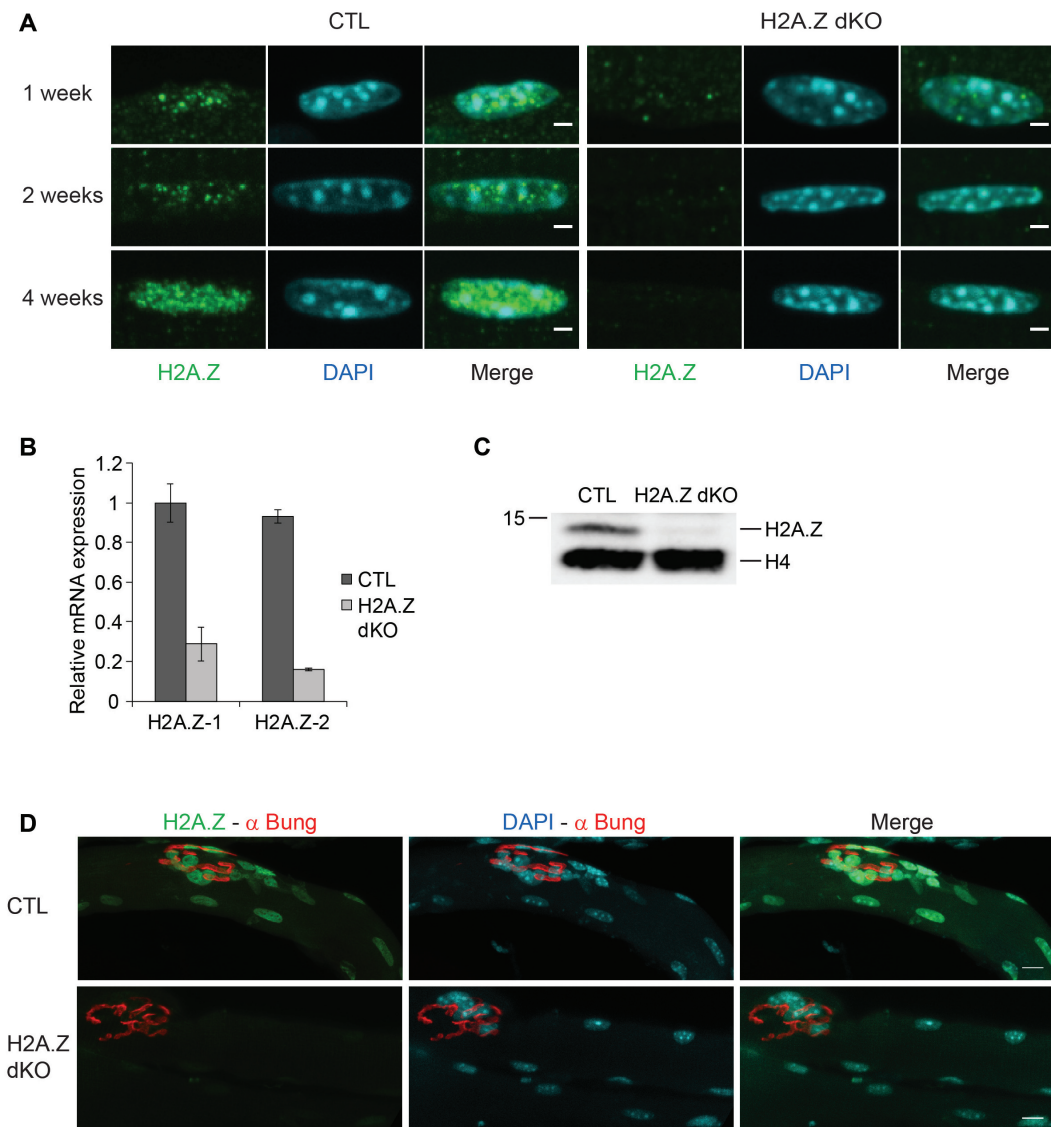
Figure 3. Validation of the H2A.Z cKO mouse model. (**A**) Immunofluorescence detection of H2A.Z on *tibialis anterior* muscle fibers from 1 week, 2 weeks and 4 weeks old CTL and H2A.Z dKO mice. DAPI was used to stain the DNA (Scale bar 2 μm). (**B**) H2A.Z-1 and H2A.Z-2 RT-qPCR of RNA isolated from the double cKO mouse strain on 7 weeks aged mice ($n = 3$). (**C**) Western blotting of H2A.Z from nuclear extracts of skeletal muscles from CTL and double cKO H2A.Z-1$^{(-/-)}$ × H2A.Z-2$^{(-/-)}$ (H2A.Z dKO) on 7 weeks old mice. H4 is used as loading control. (**D**) Immunofluorescence detection of H2A.Z on EDL muscle fibers from 7 weeks old CTL and H2A.Z dKO mice. α-bungarotoxin is used to stain the neuromuscular junction and DAPI to stain the DNA (scale bar: 10 μm).

that in muscle fibers, as in other mouse tissues (49), chromatin was the most accessible between the +1 and the −1 nucleosomes surrounding the TSS (Figure 2D).

Ablation of H2A.Z-1 and H2A.Z-2 in mouse skeletal muscle fibers

The H2A.Z-1$^{flox/flox}$:H2A.Z-2$^{flox/flox}$ mouse line was crossed with mice expressing the Cre recombinase under the control of the HSA promoter, driving expression of the Cre recombinase in post-mitotic skeletal muscle cells (30). In HSA-Cre mice, the expression of the Cre recombinase is initiated in the second half of embryonic development and reaches its plateau of expression around birth (50). The depletion of both H2A.Z in the TA muscles of 7–8 weeks

old mice was demonstrated by RT-qPCR (Figure 3B) and western blotting (Figure 3C). In both cases, the remaining signal (∼15–20%) reflects the presence of non-muscle cells e.g. fibroblasts, endothelial cells, macrophages (51). Of note, H2A.Z was below the immunofluorescence detection level in PAX7 positive satellite cells (Supplementary Figure S1). Immunofluorescence experiments were carried out to specifically visualize the decline in H2A.Z content in the nuclei of muscle fibers (Figure 3A and D). One week after birth H2A.Z levels were already significantly decreased (Figure 3A) and by post-natal week 4, H2A.Z could not be detected anymore in muscle nuclei. Consistently, 7 weeks after birth no H2A.Z could be detected in muscle nuclei whereas its expression remained unaffected in non-muscle cells (Figure 3D). For further analysis, muscles were collected seven
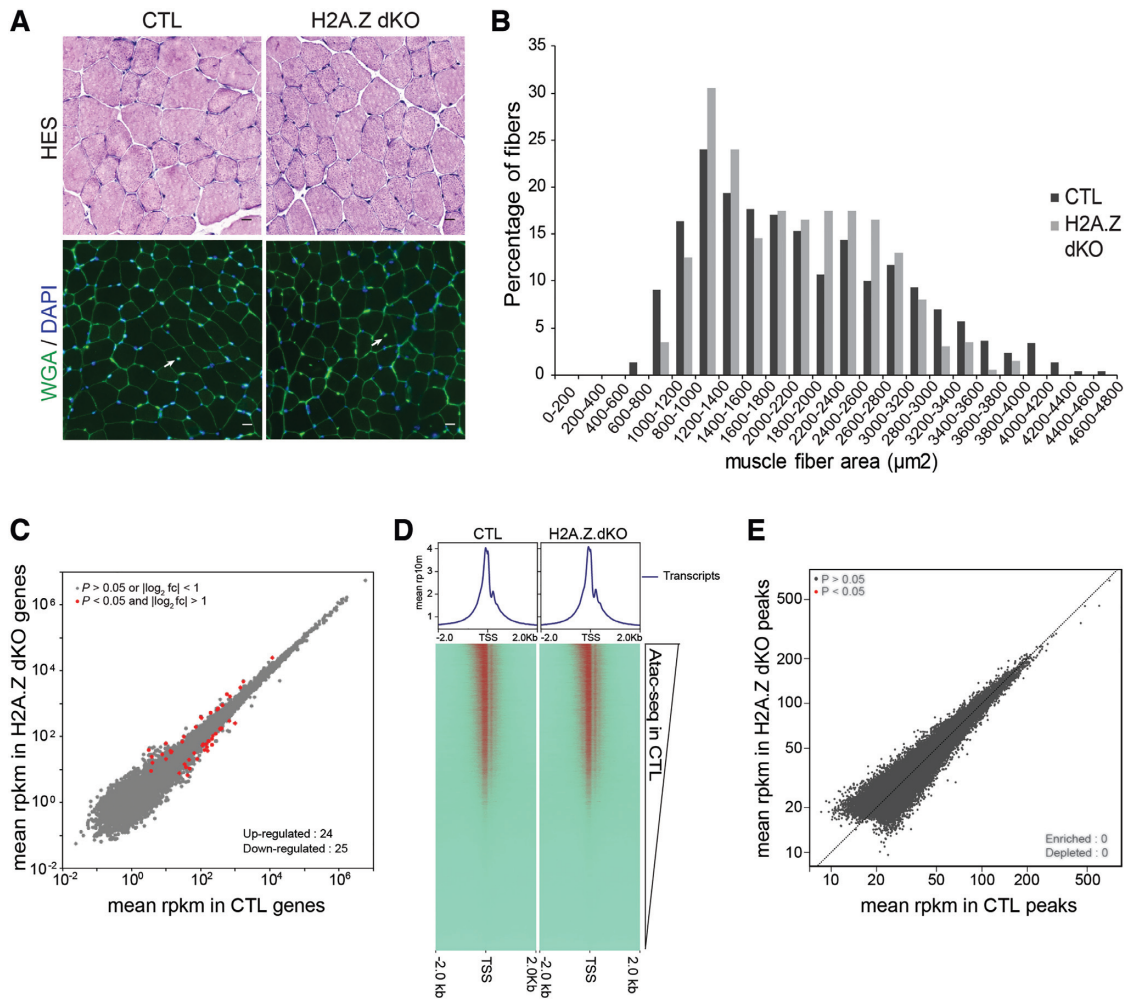
Figure 4. Characterization of the H2A.Z cKO mouse model. (**A**) Histological analysis of *tibialis anterior* muscles by Hematoxyline and Eosin (HE) and Wheat Germ Agglutinin-Lectin (WGA) staining from 7 weeks old CTL and H2A.Z dKO mice (scale bar: 20 μm, arrows indicate centronucleated fibers). (**B**) Fiber size distribution analysed from 200 myofibers of each samples. (**C**) Scatter plots comparing global gene expression levels between CTL and H2A.Z dKO cells in muscle from 7 weeks-old mice. (**D**) Heat map of the ATAC-seq signal enrichment around the transcription start sites (TSSs) in CTL and H2A.Z dKO, the TSSs being ranked according to the CTL level. (**E**) Scatter plot comparing ATAC-seq peaks enrichment in CTL and H2A.Z dKO muscles.

weeks after birth, thus several weeks after the depletion of H2A.Z (Figure 3A). Phenotypically, seven weeks old H2A.Z dKO mice were indistinguishable from control mice (CTL). Body weights were similar (with a mean of 20.7 g ± 1.3 and 21 g ± 0.7 for CTL and dKO mice, respectively; $n = 7$ for each group) and muscle histology was similar in H2A.Z dKO and CTL mice. Fibrosis, fiber type composition, and mitochondria distribution and function were identical in control and H2A.Z dKO muscles (Figure 4A, see below Supplementary Figure S5). Hematoxylin Eosin and WGA/DAPI staining were used to visualize muscle structure. Gomori's Trichrome was used to stain the connective tissue, mitochondria, rods and vacuoles. SDH-Cox and NADH staining were used to visualize the activity and distribution of the respiratory chain (52). Importantly, the distribution of fiber size (cross-sectional area) was comparable between CTL and H2A.Z dKO muscles (Figure 4B). In adult muscles, the loss of muscle fibers is usually compensated by the formation of new muscle fibers from resi-

dent adult muscle stem cells. Regenerating muscle fibers are easily detected by the central position of their nuclei since in other fibers the nuclei are located at the periphery, directly beneath the plasma membrane. We observed $0.84\% \pm 0.13$ ($n = 4$) and $0.80\% \pm 0.13$ ($n = 3$) of centronucleated fibers in H2A.Z dKO and CTL muscles, respectively. These values fit with those reported for healthy muscles (53,54) and indicate the absence of active regenerative process in H2A.Z dKO muscles. Altogether, these data reveal that H2A.Z depletion in skeletal muscle fibers does not induce any detectable alteration.

The absence of H2A.Z perturbs neither steady state gene expression nor the chromatin landscape

To evaluate the impact of H2A.Z inactivation on steady state gene expression, RNA-seq was performed on 7 weeks old CTL and H2A.Z dKO TA muscles. Analysis of the results confirmed the inactivation of both H2A.Z isoforms in H2A.Z dKO mice (Supplementary Figure S2). The tran-

scriptomes of CTL and H2A.Z dKO muscles were almost identical (Figure 4C). In the absence of H2A.Z, the expression of only 24 and 25 genes was slightly activated or repressed, respectively, and no clustering of these genes was observed (Figure 4C, Supplementary Table S3). The expression of 16 of these genes was evaluated by RT-PCR to confirm the RNA-seq results (Supplementary Figure S3). Therefore, removing H2A.Z from skeletal muscle fibers does not significantly perturb the pattern of gene expression in muscle.

When sorted according to transcriptional strength, ATAC-seq results generated identical patterns in control and H2A.Z dKO muscles (Figure 4D). This was further confirmed by directly comparing the peaks from each experiment (Figure 4E). Altogether, these results indicate that in muscle fibers nuclei, the absence of H2A.Z did not significantly change gene expression or DNA accessibility.

The absence of H2A.Z perturbs neither acute gene activation nor repression in mouse skeletal muscle

To evaluate the possibility that H2A.Z would be required to prime transcriptional changes but would be dispensable once promoters were already activated or repressed, we analysed the effect of H2A.Z inactivation upon acute changes in gene expression. For this purpose, seven weeks old CTL and H2A.Z dKO TA muscles were denervated. Denervation was carried out by section of the sciatic nerve of one hind limb. Forty eight hours after denervation, TA muscles were collected, and the contralateral TA muscles were used as innervated controls. RT-qPCR experiments showed that the strong post-denervation upregulation of *MyoD* and *Myogenin* expression took place normally in the absence of H2A.Z (Supplementary Figure S4). Note that no histological changes in denervated H2A.Z dKO mice compared to CTL mice were detected (Supplementary Figure S5).

To have a global view of the transcriptional response to denervation, RNA-seq was carried out on RNA purified from either innervated or denervated TA muscles. As expected, the expression of *Myogenin, MuSK, Acetylcholine receptor α* and *δ* and *Hdac4* was strongly upregulated (Supplementary Table S3), thus confirming that muscles responded correctly to denervation. In agreement with available data (55), the genome-wide transcriptome analysis revealed that upon denervation hundreds of genes were either upregulated (894 genes) or down-regulated (944 genes) (Figure 5A and B). Denervation induced the down-regulation of many genes involved in contractility and the up-regulation of genes involved in muscle development and inflammation (Figure 5D). In H2A.Z dKO muscles, 889 genes were up-regulated and 876 down-regulated. Up- and down-regulated genes were the same in CTL and H2A.Z dKO muscles, indicating that the vast majority of genes are normally regulated by denervation in the absence of H2A.Z (Figure 5C and Supplementary Table S3). Altogether, the depletion of H2A.Z did not significantly affect the genome–wide transcriptional response to denervation (Figure 5C). We conclude that in post-mitotic skeletal muscle cells, H2A.Z is not required to activate or to repress transcription to adapt to a particular physiological context.

H2A.Z is enriched at DNA repetitive elements but does not control their expression

Since H2A.Z is also known to be enriched at pericentromeric regions in the mouse genome, we specifically analysed repetitive sequences that represent a very high proportion of these regions (20,21). As expected, our ChIP-seq data indicated that numerous families of DNA repetitive elements were enriched in H2A.Z (Figure 6A). The families that exhibited the highest enrichment are listed in Supplementary Table S4. Of note, the majority of repeats significantly enriched in H2A.Z (log_2 enrichment > 0.5 and *P* value $< 10^{-2}$) belonged to the simple repeats and to the endogenous retrovirus classes of repetitive elements. This suggested that H2A.Z might be involved in the control of the expression of these repetitive DNA elements. To test this hypothesis, we analysed how the absence of H2A.Z affected the expression of repetitive DNA elements in innervated and denervated muscles of seven weeks old mice (Figure 6). The expression of repetitive elements was indistinguishable in CTL and H2A.Z dKO innervated muscle (Figure 6B). Interestingly, denervation altered the expression of several types of repetitive elements in control muscles. 72 families were up-regulated and 3 were down-regulated 48 hours after denervation (Figure 6C). These changes were similar in H2A.Z dKO muscles (Figure 6D, E, Supplementary Table S5). The MLTH1 and RLTR6 families of repetitive elements were among the most up-regulated by denervation. H2A.Z inactivation affected neither their expression in innervated muscle nor their activation in denervated muscle (Figure 6E). Taken as a whole, these results indicate that H2A.Z is neither required for normal expression nor for the activation of repetitive DNA elements.

DISCUSSION

The goal of this study was to evaluate the transcriptional role of H2A.Z in post-mitotic tissues *in vivo*. As model system, we first isolated MEF cells derived from H2AZ.1$^{flox/flox}$:H2AZ.2$^{flox/flox}$ mice. In cycling MEFs, H2A.Z was depleted in less than two days after adeno-Cre infection, and many genes were up- and down-regulated (Figure 1F and data not shown) fitting with the literature (25,56,57). We next sought to avoid a possible influence of the cell cycle on gene expression in the absence of H2A.Z. We chose an *in vivo* approach in skeletal muscle because it provides access to long lived post-mitotic cells in which Cre recombinase expression can be efficiently targeted, and where consequences can be analysed several weeks after gene inactivation. In addition, denervation provides a convenient means to rapidly change the transcriptional program of the targeted cells.

ChIP-seq analysis confirmed that in skeletal muscle fibers, H2A.Z was enriched at transcriptional start sites and on regulatory elements as previously described in other systems (15,17,18,23). To specifically inactivate H2A.Z in the skeletal muscle fibers of H2A.Z-1$^{flox/flox}$:H2A.Z-2$^{flox/flox}$ mice, HSA-Cre mice were used. This mouse line is probably the best characterized muscle specific Cre-driver mouse, and allows for the selective targeting of post-mitotic skeletal muscle cells (30).
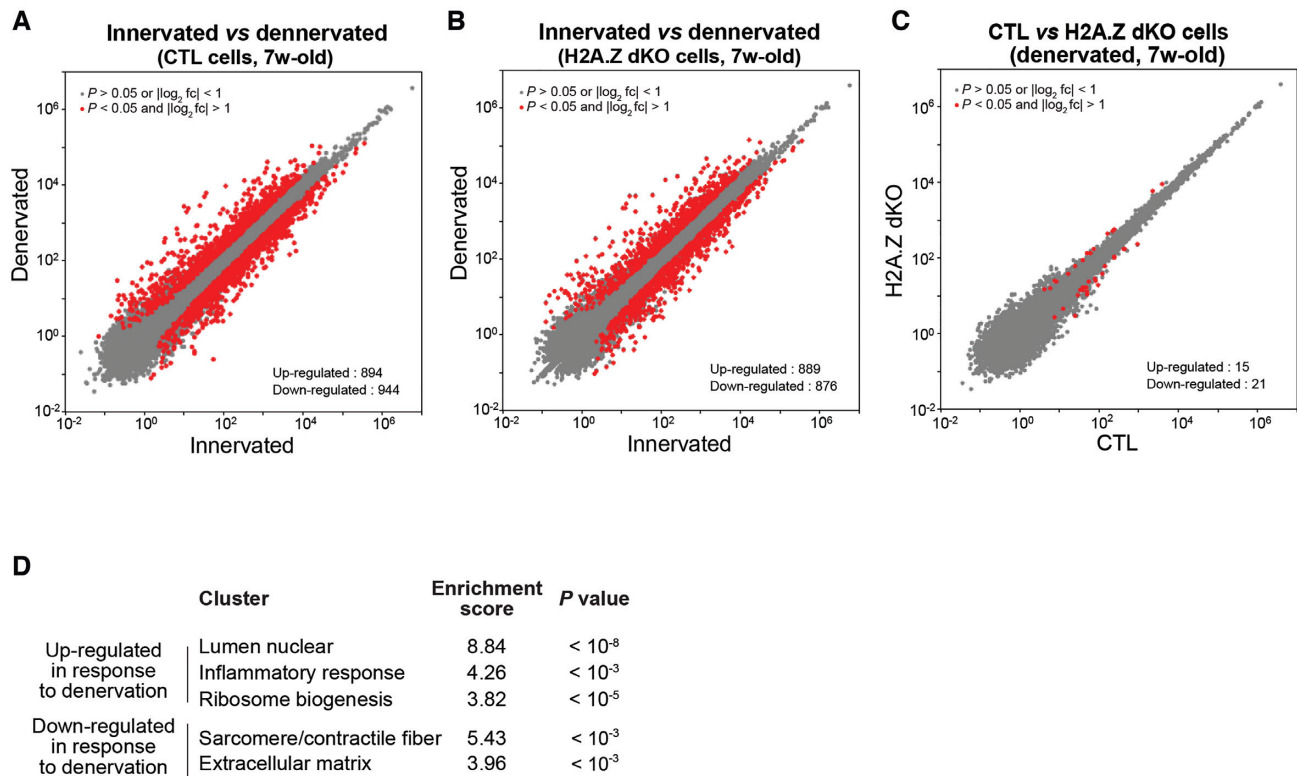
Figure 5. Characterization of the H2A.Z cKO under acute transcriptional response. (A, B) Scatter plots comparing global gene expression levels between innervated and denervated cells (in 7 weeks-old mice) in the presence (**A**) or in the absence (**B**) of H2A.Z. (**C**) Scatter plots comparing global gene expression levels 48h after denervation between CTL and H2A.Z dKO muscle cells of 7 weeks-old mice. (**D**) Functional annotation clustering of differentially expressed genes in response to denervation.

Skeletal muscles contain a large variety of cell types (fibroblasts, satellite cells, macrophages, endothelial cells etc.) (51). The Human Skeletal Actin promoter drives the expression of the Cre recombinase specifically in differentiated muscle cells. When performing muscle extracts from the whole tissue, non muscle cells such as fibroblasts are inevitably present. These cells represent less than 20% of the muscle tissue but they are sufficiently represented to generate detectable expression of inactivated genes in muscle extracts. This is true for H2A.Z dKO muscles and for all muscle specific inactivation of ubiquitously expressed genes (53,54,58–60). By allowing for visualization of individual nuclei, immunofluorescence was the best way to evaluate the efficiency of H2A.Z knock-down in muscle fibers. In H2A.Z dKO muscles, H2A.Z staining had already decreased below the detection level by 2 weeks of age and H2A.Z remained undetectable in muscle fibers at later timepoints. H2A.Z immunostaining indicated that quiescent satellite cells contained very low levels of H2A.Z compared to muscle fibers. However, H2A.Z has been described to be required for the differentiation of myoblasts into myotubes (61,62), and our observations also show that cultured myoblasts strongly express H2A.Z during differentiation (data not shown). These results suggest that upon activation, H2A.Z expression is rapidly up-regulated in satellite cells.

When analysed seven weeks after birth, H2A.Z dKO mice and H2A.Z dKO muscles did not show any detectable alteration (Figure 4A and B). Strikingly, RNA-seq analysis revealed no significant effect of H2A.Z depletion on the transcriptomic profile of H2A.Z dKO muscles. It is highly improbable that the presence of non-muscle cells in the muscle samples could have masked a possible effect. Muscle fibers express many muscle specific genes. The presence of non-muscle RNA in the samples should not affect their expression fold change. If the contribution of non-muscle cells had been sufficient to mask variations in expression, the RNA-seq would have generated at least two different groups of results: muscle specific genes would have shown variations whereas ubiquitously expressed genes would not have been affected. We therefore conclude that neither the presence of non-muscle cells nor the presence of satellite cells significantly impacted the results.

Induction of a new transcriptional program by denervation was also not perturbed by the absence of H2A.Z. Of note, upon denervation only muscle fibers adopt a specific transcriptional program and many up-regulated and down-regulated genes are muscle specific (MyoD, Myogenin, AChR subunits, MuSK etc.). In addition, muscle stem cells (e.g. the satellite cells) are not activated in the experimental time frame we used (63,64). This was confirmed by the absence of PAX7 up-regulation in control denervated mice (log$_2$ fold change between the innervated and denervated situation of 0.29 ± 0.22 and -0.007 ± 0.98 in CTL and H2A.Z dKO muscles, respectively).

H2A.Z is also preferentially enriched at regulatory elements such as enhancers and CTCF-binding sites, which
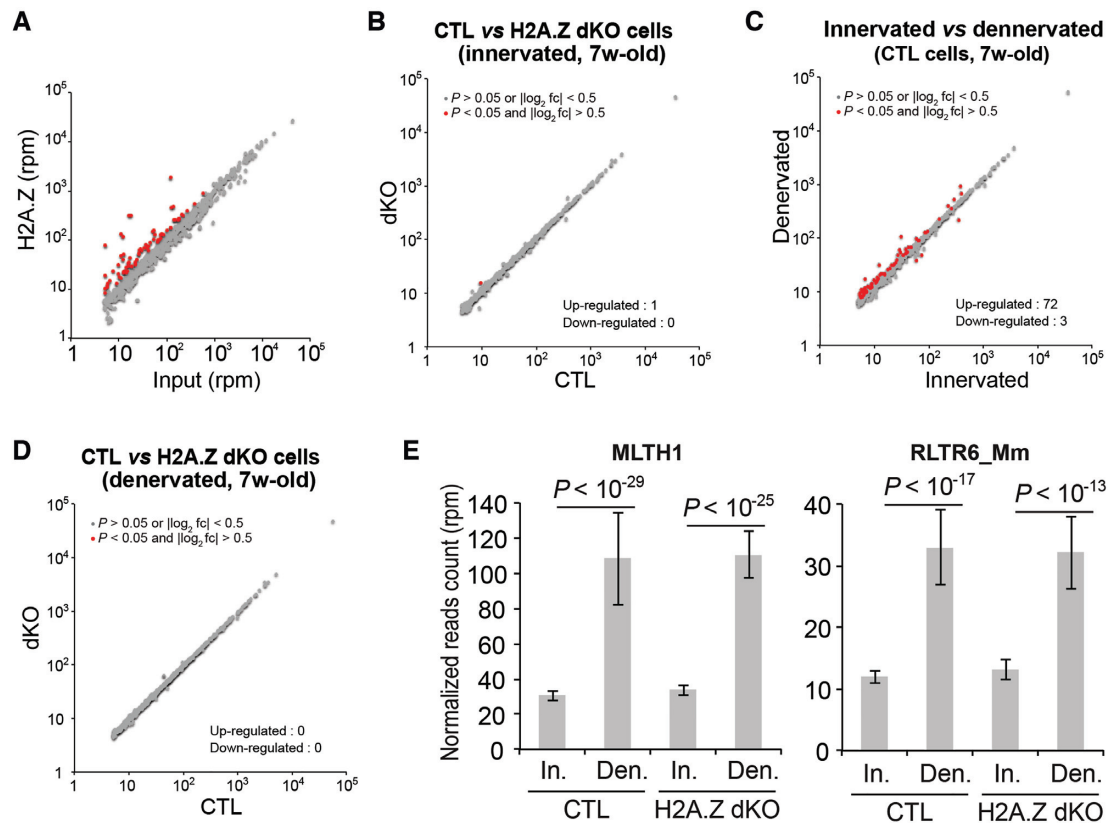
Figure 6. H2A.Z at DNA repetitive elements. (**A**) Scatter plot showing the average enrichment of H2A.Z in DNA repeat families. (**B**) Scatter plots comparing global transcription of repetitive elements between CTL and H2A.Z dKO myofibers in innervated muscle of 7 weeks-old mice. (**C**) Scatter plots comparing global transcription of repetitive elements in innervated and denervated muscle cells (7 weeks-old mice) in the presence of H2A.Z. (**D**) Scatter plots comparing global transcription of repetitive elements between CTL and H2A.Z dKO myofibers in denervated muscle of 7 weeks-old mice. (**E**) Bar graphs representing the expression level of the MLTH1 and RLTR6_Mm retroelements, the two most overexpressed retroelements in response to denervation.

mark insulator sites in the genome (17). ATAC-seq results would have shown changes in chromatin accessibility if H2A.Z depletion had perturbed enhancers or insulators function. We can therefore conclude that H2A.Z is not required for the function of enhancers and insulators in muscle fibers

Our results demonstrate that H2A.Z does not play a prominent role in transcription, but it is still an essential protein in cycling cells. H2A.Z is enriched at centric and pericentromeric heterochromatin (21,65,66), and it is also, somehow, involved in mitosis (21) and in DNA replication (28,29). If H2A.Z has key roles in organizing the centrosome or other chromatin loci crucial for mitosis or in DNA replication, these functions are important enough to lead to cell death when perturbed. The fact that none of these functions are required in post-mitotic cells would explain why H2A.Z is not an essential protein in post-mitotic muscle cells.

It would be interesting to investigate the nucleosome composition at TSS in the absence of H2A.Z. Four non-exclusive possibilities would fit with our data. The first, and most likely hypothesis, is that H2A.Z is replaced by canonical H2A. H2A expression is stronger during S phase (67), however, low level of H2A expression is probably sufficient in post-mitotic cells. This is the case for histone H4, for

which there is no known variant in the mouse genome (to our knowledge H4 has a variant only in hominids (4)). If H4 is expressed at low levels from one of the histone clusters, H2A might be as well. The second possibility is that H2A.Z is replaced by another H2A variant. There are many H2A variants which can be incorporated in nucleosomes. However, their expression was not upregulated in H2A.Z dKO muscles. The third possibility is that H2A.Z is not replaced by another histone, thus creating an incomplete nucleosome e.g. a tetrasome at the TSS (see (68)) or even gaps in chromatin if the tetrasome is too unstable. However, ATAC-seq results did not reveal any increase in chromatin accessibility, arguing against this hypothesis. The fourth possibility, which cannot be excluded, would be that a subset of H2A.Z exists, that is more stable than the bulk of H2AZ molecules, and is sufficient to assume genome wide transcriptional functions of H2A.Z seven weeks after ablation of H2A.Z expression. This stable fraction would probably correspond to H2A.Z molecules present in non-remodeled nucleosomes, such as those present on condensed genomic regions, which would constitute a pool of several tens of thousands of molecules. Immunostaining would probably detect such amounts of H2A.Z.

Altogether, the most likely explanation is that canonical H2A replaces missing H2A.Z molecules, but completely

ruling out the other possibilities will require further in depth investigations.

It has long been thought that since H2A.Z was enriched at TSS, it was playing an active role in transcriptional regulation. Our results showing normal gene expression and regulation in post-mitotic muscle cells challenge this view. Almost all data available so far were obtained using cycling cells and could not rule out the possibility that H2A.Z functions in processes other than transcription. A role in replication or DNA repair could easily explain why H2A.Z total KO in mouse is lethal during early embryonic development. Our results suggest that the requirement of H2A.Z for cellular viability *in vivo* is not linked to transcription. Alternatively, a differential involvement of H2A.Z in transcription in cycling and post-mitotic cells could be envisaged. Indeed, previous studies have demonstrated specific developmental functions of H2A.Z via the regulation of the accessibility of specific promoters (25). Even though, H2A.Z accumulation at active TSS and regulatory elements with no apparent function in post-mitotic cells would still be puzzling.

If not required for a specific transcriptional function, the accumulation of H2A.Z at TSS and regulatory regions is intriguing. A simple explanation of this phenomenon could be provided by the fact that overall, H2A.Z accumulates at sites where nucleosome turnover is high. H2A.Z could be preferentially incorporated in new nucleosomes at these sites because it is more available than its canonical counterpart (which is mainly expressed during the S phase). H2A.Z would therefore be used to locally reconstitute chromatin and to protect the DNA from damage without playing an active role in gene expression (69). Altogether, these results suggest that H2A.Z is rather a marker than an active driver of transcription. Recently, several reports on the essential variant H3.3 similarly claimed that it is dispensable for transcription (35,69). This raises the question of the role of histone variants in transcriptional regulation as a whole.

DATA AVAILABILITY

The ChIP-seq and RNA-seq datasets have been deposited in the Gene Expression Omnibus (GEO; http://www.ncbi.nlm.nih.gov/geo/) under the accession number GSE111576.

SUPPLEMENTARY DATA

Supplementary Data are available at NAR Online.

ACKNOWLEDGEMENTS

FUNDING

REFERENCES

1. Maze,I., Noh,K.-M., Soshnev,A.A. and Allis,C.D. (2014) Every amino acid matters: essential contributions of histone variants to mammalian development and disease. *Nat. Rev. Genet.*, **15**, 259–271.
2. Van Holde,K.E. (1989) Chromatin. Series in molecular biology. Springer-Verlag, New York. 1988. 530 pp. $98.00. *J. Mol. Recognit.*, **2**, i.
3. Talbert,P.B. and Henikoff,S. (2017) Histone variants on the move: substrates for chromatin dynamics. *Nat. Rev. Mol. Cell Biol.*, **18**, 115–126.
4. Long,M., Sun,X., Shi,W., Yanru,A., Leung,S.T.C., Ding,D., Cheema,M.S., MacPherson,N., Nelson,C.J., Ausio,J. *et al.* (2019)A novel histone H4 variant H4G regulates rDNA transcription in breast cancer. *Nucleic Acids Res.*, **47**, 8399–8409.
5. Cheema,M.S. and Ausió,J. (2015) The structural determinants behind the epigenetic role of histone variants. *Genes*, **6**, 685–713.
6. Ausió,J. (2006) Histone variants–the structure behind the function. *Brief. Funct. Genomic. Proteomic.*, **5**, 228–243.
7. Thambirajah,A.A., Li,A., Ishibashi,T. and Ausió,J. (2009) New developments in post-translational modifications and functions of histone H2A variants. *Biochem. Cell Biol.*, **87**, 7–17.
8. Zink,L.-M. and Hake,S.B. (2016) Histone variants: nuclear function and disease. *Curr. Opin. Genet. Dev.*, **37**, 82–89.
9. Boulard,M., Bouvet,P., Kundu,T.K. and Dimitrov,S. (2007) Histone variant nucleosomes: structure, function and implication in disease. *Subcell. Biochem.*, **41**, 71–89.
10. Corujo,D. and Buschbeck,M. (2018) Post-Translational modifications of H2A histone variants and their role in cancer. *Cancers*, **10**, 59.
11. Sarma,K. and Reinberg,D. (2005) Histone variants meet their match. *Nat. Rev. Mol. Cell Biol.*, **6**, 139–149.
12. Eirín-López,J.M., González-Romero,R., Dryhurst,D., Ishibashi,T. and Ausió,J. (2009) The evolutionary differentiation of two histone H2A.Z variants in chordates (H2A.Z-1 and H2A.Z-2) is mediated by a stepwise mutation process that affects three amino acid residues. *BMC Evol. Biol.*, **9**, 31.
13. Dryhurst,D., Ishibashi,T., Rose,K.L., Eirín-López,J.M., McDonald,D., Silva-Moreno,B., Veldhoen,N., Helbing,C.C., Hendzel,M.J., Shabanowitz,J. *et al.* (2009) Characterization of the histone H2A.Z-1 and H2A.Z-2 isoforms in vertebrates. *BMC Biol.*, **7**, 86.
14. Faast,R., Thonglairoam,V., Schulz,T.C., Beall,J., Wells,J.R.E., Taylor,H., Matthaei,K., Rathjen,P.D., Tremethick,D.J. and Lyons,I. (2001) Histone variant H2A.Z is required for early mammalian development. *Curr. Biol.*, **11**, 1183–1187.

15. Obri,A., Ouararhni,K., Papin,C., Diebold,M.-L., Padmanabhan,K., Marek,M., Stoll,I., Roy,L., Reilly,P.T., Mak,T.W. *et al.* (2014) ANP32E is a histone chaperone that removes H2A.Z from chromatin. *Nature*, **505**, 648–653.

16. Latrick,C.M., Marek,M., Ouararhni,K., Papin,C., Stoll,I., Ignatyeva,M., Obri,A., Ennifar,E., Dimitrov,S., Romier,C. *et al.* (2016) Molecular basis and specificity of H2A.Z-H2B recognition and deposition by the histone chaperone YL1. *Nat. Struct. Mol. Biol.*, **23**, 309–316.

17. Barski,A., Cuddapah,S., Cui,K., Roh,T.-Y., Schones,D.E., Wang,Z., Wei,G., Chepelev,I. and Zhao,K. (2007) High-resolution profiling of histone methylations in the human genome. *Cell*, **129**, 823–837.

18. Nekrasov,M., Soboleva,T.A., Jack,C. and Tremethick,D.J. (2013) Histone variant selectivity at the transcription start site: H2A.Z or H2A.Lap1. *Nucleus*, **4**, 431–437.

19. Nekrasov,M., Amrichova,J., Parker,B.J., Soboleva,T.A., Jack,C., Williams,R., Huttley,G.A. and Tremethick,D.J. (2012) Histone H2A.Z inheritance during the cell cycle and its impact on promoter organization and dynamics. *Nat. Struct. Mol. Biol.*, **19**, 1076–1083.

20. Sarcinella,E., Zuzarte,P.C., Lau,P.N.I., Draker,R. and Cheung,P. (2007) Monoubiquitylation of H2A.Z distinguishes its association with euchromatin or facultative heterochromatin. *Mol. Cell Biol.*, **27**, 6457–6468.

21. Greaves,I.K., Rangasamy,D., Ridgway,P. and Tremethick,D.J. (2007) H2A.Z contributes to the unique 3D structure of the centromere. *Proc. Natl. Acad. Sci. U.S.A.*, **104**, 525–530.

22. Boyarchuk,E., Filipescu,D., Vassias,I., Cantaloube,S. and Almouzni,G. (2014) The histone variant composition of centromeres is controlled by the pericentric heterochromatin state during the cell cycle. *J. Cell Sci.*, **127**, 3347–3359.

23. Weber,C.M., Henikoff,J.G. and Henikoff,S. (2010) H2A.Z nucleosomes enriched over active genes are homotypic. *Nat. Struct. Mol. Biol.*, **17**, 1500–1507.

24. Svensson,J.P., Shukla,M., Menendez-Benito,V., Norman-Axelsson,U., Audergon,P., Sinha,I., Tanny,J.C., Allshire,R.C. and Ekwall,K. (2015) A nucleosome turnover map reveals that the stability of histone H4 Lys20 methylation depends on histone recycling in transcribed chromatin. *Genome Res.*, **25**, 872–883.

25. Giaimo,B.D., Ferrante,F., Vallejo,D.M., Hein,K., Gutierrez-Perez,I., Nist,A., Stiewe,T., Mittler,G., Herold,S., Zimmermann,T. *et al.* (2018) Histone variant H2A.Z deposition and acetylation directs the canonical Notch signaling response. *Nucleic Acids Res.*, **46**, 8197–8215.

26. Domaschenz,R., Kurscheid,S., Nekrasov,M., Han,S. and Tremethick,D.J. (2017) The histone variant H2A.Z is a master regulator of the Epithelial-Mesenchymal transition. *Cell Rep.*, **21**, 943–952.

27. Rangasamy,D., Greaves,I. and Tremethick,D.J. (2004) RNA interference demonstrates a novel role for H2A.Z in chromosome segregation. *Nat. Struct. Mol. Biol.*, **11**, 650–655.

28. Cayrou,C., Ballester,B., Peiffer,I., Fenouil,R., Coulombe,P., Andrau,J.-C., van Helden,J. and Méchali,M. (2015) The chromatin environment shapes DNA replication origin organization and defines origin classes. *Genome Res.*, **25**, 1873–1885.

29. Long,H., Zhang,L., Lv,M., Wen,Z., Zhang,W., Chen,X., Zhang,P., Li,T., Chang,L., Jin,C. *et al.* (2019) H2A.Z facilitates licensing and activation of early replication origins. *Nature*, **577**, 576–581.

30. Miniou,P., Tiziano,D., Frugier,T., Roblot,N., Meur,M.L. and Melki,J. (1999) Gene targeting restricted to mouse striated muscle lineage. *Nucleic Acids Res.*, **27**, e27.

31. Raffaello,A., Laveder,P., Romualdi,C., Bean,C., Toniolo,L., Germinario,E., Megighian,A., Danieli-Betto,D., Reggiani,C. and Lanfranchi,G. (2006) Denervation in murine fast-twitch muscle: short-term physiological changes and temporal expression profiling. *Physiol. Genomics*, **25**, 60–74.

32. Méjat,A., Ramond,F., Bassel-Duby,R., Khochbin,S., Olson,E.N. and Schaeffer,L. (2005) Histone deacetylase 9 couples neuronal activity to muscle chromatin acetylation and gene expression. *Nat. Neurosci.*, **8**, 313–321.

33. Thomas,J.-L., Moncollin,V., Ravel-Chapuis,A., Valente,C., Corda,D., Méjat,A. and Schaeffer,L. (2015) PAK1 and CtBP1 regulate the coupling of neuronal activity to muscle chromatin and gene expression. *Mol. Cell Biol.*, **35**, 4110–4120.

34. Papin,C., Ibrahim,A., Gras,S.L., Velt,A., Stoll,I., Jost,B., Menoni,H., Bronner,C., Dimitrov,S. and Hamiche,A. (2017) Combinatorial DNA methylation codes at repetitive elements. *Genome Res.*, **27**, 934–946.

35. Ors,A., Papin,C., Favier,B., Roulland,Y., Dalkara,D., Ozturk,M., Hamiche,A., Dimitrov,S. and Padmanabhan,K. (2017) Histone H3.3 regulates mitotic progression in mouse embryonic fibroblasts. *Biochem. Cell Biol.*, **95**, 491–499.

36. Trapnell,C., Pachter,L. and Salzberg,S.L. (2009) TopHat: discovering splice junctions with RNA-Seq. *Bioinformatics*, **25**, 1105–1111.

37. Anders,S. and Huber,W. (2010) Differential expression analysis for sequence count data. *Genome Biol.*, **11**, R106.

38. Buenrostro,J., Wu,B., Chang,H. and Greenleaf,W. (2015) ATAC-seq: a method for assaying chromatin accessibility Genome-Wide. *Curr. Protoc. Mol. Biol. Ed. Frederick M Ausubel Al*, **109**, 21.29.1–21.29.9.

39. Bolger,A.M., Lohse,M. and Usadel,B. (2014) Trimmomatic: a flexible trimmer for Illumina sequence data. *Bioinforma. Oxf. Engl.*, **30**, 2114–2120.

40. Li,H., Handsaker,B., Wysoker,A., Fennell,T., Ruan,J., Homer,N., Marth,G., Abecasis,G., Durbin,R. and 1000 Genome Project Data Processing Subgroup (2009) The Sequence Alignment/Map format and SAMtools. *Bioinforma. Oxf. Engl.*, **25**, 2078–2079.

41. Tarasov,A., Vilella,A.J., Cuppen,E., Nijman,I.J. and Prins,P. (2015) Sambamba: fast processing of NGS alignment formats. *Bioinforma. Oxf. Engl.*, **31**, 2032–2034.

42. Zhang,Y., Liu,T., Meyer,C.A., Eeckhoute,J., Johnson,D.S., Bernstein,B.E., Nusbaum,C., Myers,R.M., Brown,M., Li,W. *et al.* (2008) Model-based Analysis of ChIP-Seq (MACS). *Genome Biol.*, **9**, R137.

43. Buenrostro,J.D., Giresi,P.G., Zaba,L.C., Chang,H.Y. and Greenleaf,W.J. (2013) Transposition of native chromatin for fast and sensitive epigenomic profiling of open chromatin, DNA-binding proteins and nucleosome position. *Nat. Methods*, **10**, 1213–1218.

44. Amemiya,H.M., Kundaje,A. and Boyle,A.P. (2019) The ENCODE blacklist: identification of problematic regions of the genome. *Sci. Rep.*, **9**, 1–5.

45. Quinlan,A.R. and Hall,I.M. (2010) BEDTools: a flexible suite of utilities for comparing genomic features. *Bioinformatics*, **26**, 841–842.

46. Love,M.I., Huber,W. and Anders,S. (2014) Moderated estimation of fold change and dispersion for RNA-seq data with DESeq2. *Genome Biol.*, **15**, 550.

47. Ramírez,F., Ryan,D.P., Grüning,B., Bhardwaj,V., Kilpert,F., Richter,A.S., Heyne,S., Dündar,F. and Manke,T. (2016) deepTools2: a next generation web server for deep-sequencing data analysis. *Nucleic Acids Res.*, **44**, W160–W165.

48. Nekrasov,M., Soboleva,T.A., Jack,C. and Tremethick,D.J. (2013) Histone variant selectivity at the transcription start site: H2A.Z or H2A.Lap1. *Nucleus*, **4**, 431–437.

49. Liu,C., Wang,M., Wei,X., Wu,L., Xu,J., Dai,X., Xia,J., Cheng,M., Yuan,Y., Zhang,P. *et al.* (2019) An ATAC-seq atlas of chromatin accessibility in mouse tissues. *Sci. Data*, **6**, 65.

50. Rao,P. and Monks,D.A. (2009) A tetracycline-inducible and skeletal muscle-specific Cre recombinase transgenic mouse. *Dev. Neurobiol.*, **69**, 401–406.

51. Giordani,L., He,G.J., Negroni,E., Sakai,H., Law,J.Y.C., Siu,M.M., Wan,R., Corneau,A., Tajbakhsh,S., Cheung,T.H. *et al.* (2019) High-dimensional single-cell cartography reveals novel skeletal Muscle-Resident cell populations. *Mol. Cell*, **74**, 609–621.

52. Pál,E. (2015) Skeletal Muscle Pathology in Mitochondrial Diseases. *Mitochondrial Diseases and Therapy*, 1–16.

53. Risson,V., Mazelin,L., Roceri,M., Sanchez,H., Moncollin,V., Corneloup,C., Richard-Bulteau,H., Vignaud,A., Baas,D., Defour,A. *et al.* (2009) Muscle inactivation of mTOR causes metabolic and dystrophin defects leading to severe myopathy. *J. Cell Biol.*, **187**, 859–874.

54. Zhang,Q., Duplany,A., Moncollin,V., Mouradian,S., Goillot,E., Mazelin,L., Gauthier,K., Streichenberger,N., Angleraux,C., Chen,J. *et al.* (2019) Lack of muscle mTOR kinase activity causes early onset myopathy and compromises whole-body homeostasis. *J. Cachexia Sarcopenia Muscle*, **10**, 35–53.

55. Magnusson,C., Svensson,A., Christerson,U. and Tågerud,S. (2005) Denervation-induced alterations in gene expression in mouse skeletal muscle. *Eur. J. Neurosci.*, **21**, 577–580.

56. Li,B., Pattenden,S.G., Lee,D., Gutiérrez,J., Chen,J., Seidel,C., Gerton,J. and Workman,J.L. (2005) Preferential occupancy of histone

variant H2AZ at inactive promoters influences local histone modifications and chromatin remodeling. *Proc. Natl. Acad. Sci. U.S.A.*, **102**, 18385–18390.

57. Zhang,H., Roberts,D.N. and Cairns,B.R. (2005) Genome-wide dynamics of Htz1, a histone H2A variant that poises repressed/basal promoters for activation through histone loss. *Cell*, **123**, 219–231.

58. Bentzinger,C.F., Romanino,K., Cloëtta,D., Lin,S., Mascarenhas,J.B., Oliveri,F., Xia,J., Casanova,E., Costa,C.F., Brink,M. *et al.* (2008) Skeletal muscle-specific ablation of raptor, but not of rictor, causes metabolic changes and results in muscle dystrophy. *Cell Metab.*, **8**, 411–424.

59. Castets,P., Rion,N., Théodore,M., Falcetta,D., Lin,S., Reischl,M., Wild,F., Guérard,L., Eickhorst,C., Brockhoff,M. *et al.* (2019) mTORC1 and PKB/Akt control the muscle response to denervation by regulating autophagy and HDAC4. *Nat. Commun.*, **10**, 3187.

60. Zhao,K., Shen,C., Lu,Y., Huang,Z., Li,L., Rand,C.D., Pan,J., Sun,X.-D., Tan,Z., Wang,H. *et al.* (2017) Muscle Yap Is a Regulator of Neuromuscular Junction Formation and Regeneration. *J. Neurosci.*, **37**, 3465–3477.

61. Cuadrado,A., Corrado,N., Perdiguero,E., Lafarga,V., Muñoz-Canoves,P. and Nebreda,A.R. (2010) Essential role of p18Hamlet/SRCAP-mediated histone H2A.Z chromatin incorporation in muscle differentiation. *EMBO J.*, **29**, 2014–2025.

62. Law,C. and Cheung,P. (2015) Expression of non-acetylatable H2A.Z in myoblast cells blocks myoblast differentiation through disruption of MyoD expression. *J. Biol. Chem.*, **290**, 13234–13249.

63. Dedkov,E.I., Borisov,A.B., Wernig,A. and Carlson,B.M. (2003) Aging of skeletal muscle does not affect the response of satellite cells to denervation. *J. Histochem. Cytochem.*, **51**, 853–863.

64. Kuschel,R., Yablonka-Reuveni,Z. and Bornemann,A. (1999) Satellite cells on isolated myofibers from normal and denervated adult rat muscle. *J. Histochem. Cytochem.*, **47**, 1375–1383.

65. Rangasamy,D., Berven,L., Ridgway,P. and Tremethick,D.J. (2003) Pericentric heterochromatin becomes enriched with H2A.Z during early mammalian development. *EMBO J.*, **22**, 1599–1607.

66. Ryan,D.P. and Tremethick,D.J. (2018) The interplay between H2A.Z and H3K9 methylation in regulating HP1α binding to linker histone-containing chromatin. *Nucleic Acids Res.*, **46**, 9353–9366.

67. Harris,M.E., Böhni,R., Schneiderman,M.H., Ramamurthy,L., Schümperli,D. and Marzluff,W.F. (1991) Regulation of histone mRNA in the unperturbed cell cycle: evidence suggesting control at two posttranscriptional steps. *Mol. Cell Biol.*, **11**, 2416–2424.

68. Luger,K., Dechassa,M.L. and Tremethick,D.J. (2012) New insights into nucleosome and chromatin structure: an ordered state or a disordered affair? *Nat. Rev. Mol. Cell Biol.*, **13**, 436–447.

69. Jang,C.-W., Shibata,Y., Starmer,J., Yee,D. and Magnuson,T. (2015) Histone H3.3 maintains genome integrity during mammalian development. *Genes Dev.*, **29**, 1377–1392.